Journal of Research and Applications in Mechanical Engineering
ISSN: 2229-2152 (Print); 2697-424x (Online)
(2026) Vol. 14, No. 1, Paper No. JRAME 26-14-014
[DOI: 10.14456/ jrame.2026.14]

Research Article

Microstructural and Mechanical Evaluation of Dissimilar AISI 304 and 430 Stainless Steel Welds Created with GMAW and ER308L Filler Metal

M.K. Mishra[1]
A. Chandola[2,*]
[1] *Department of Mechanical Engineering, School of Engineering, Dayananda Sagar University, Harohalli, 562112, India*
[2] *School of Computer Science & Engineering, RV University, Bengaluru, 560059, India*

Received 8 November 2024
Revised 14 February 2025
Accepted 13 April 2025

Abstract:
The fusion of dissimilar materials—specifically AISI 430 Ferritic Stainless Steel (FSS) and AISI 304 Austenitic Stainless Steel (ASS)—was accomplished using the Gas Metal Arc Welding (GMAW) process, with ER308L serving as the filler material. The experimental design was based on the Taguchi approach, which used L27 Orthogonal Arrays to systematically alter welding parameters. The impact of these factors was assessed using Analysis of Variance (ANOVA). Mechanical properties such as tensile strength, hardness, and penetration depth were evaluated, revealing that the ultimate tensile strength reached 630.7 MPa of the welded samples. The hardness of weld zone peaked at 310 HV, exceeding the base metals due to martensitic transformation and grain refinement. Optimal welding parameters were determined at 190 A, 32 V and 40 cm/min. Microstructural investigations were conducted using Field Emission Scanning Electron Microscopy (FESEM), Energy Dispersive X-ray Spectroscopy (EDX), X-ray Diffraction (XRD), and Optical Microscopy. XRD presented dominant martensitic peaks at 44.88°, 65.34°, 82.06° and 99.52°, corresponding to (110), (200), (211) and (220) crystallographic planes. EDS revealed the phase transformation was significantly influenced by the diffusion of Cr (19.20 %), Ni (6.31 %) and C (4.52 %). The findings indicated the weld bead's shape as well as the consequences of microstructural changes. Constant current and voltage, faster welding rates resulted in increased penetration depth, and the weld zone was harder than both the base metal and the HAZ.

Keywords: *Welding Parameters, Ferritic Stainless Steel (FSS), Austenitic Stainless Steel (ASS), Mechanical Properties, GMAW*

1. Introduction

Welding has become a crucial metal joining technique, allowing for the fusion of nearly any metal components into a unified structure [1]. This process, whether used in fabrication or sculpting, involves the merging of two or more materials—whether identical or different—into a single entity. Dissimilar metal joints find applications across various industries, including automotive manufacturing, nuclear power plants, and coal-fired boilers [2]. The use of dissimilar material welding has recently acquired popularity in a variety of industries, including automotive, manufacturing, chemical, pharmaceutical, nuclear, aerospace, maritime, beverage, textile, food processing, and paper. Joining dissimilar materials can result in distinct mechanical properties, enabling for weight and production cost reductions while maintaining safety and structural integrity [3].

* Corresponding author: A. Chandola
E-mail address: achandola95@gmail.com

Various welding methods are employed to join dissimilar materials, including gas tungsten arc welding (GTAW), submerged arc welding (SAW), gas metal arc welding (GMAW), pressure welding, explosion welding (EXW), friction welding, fusion welding, diffusion. Welding, brazing and soldering [4]. The successful integration of various welding processes is critical for producing high-quality welds in different materials.

GMAW is a robust welding method that considerably improves the mechanical properties of welded materials. Since 1950, this technology has been extensively used in the manufacturing of various ferrous and non-ferrous metals due to its high efficiency, cost-effectiveness, ease of use and minimal material inclusion [5]. The technique is adaptable and can be carried out semi-automatically or totally autonomously, with minimal alloy element loss during welding [6,7]. GMAW is suitable for welding stainless steel, carbon steel, copper, and aluminium if the electrode, shielding gas, and welding location are suitably chosen [8, 9].

Stainless steels (SS) are alloys of iron containing 8-25% nickel and12-30% chromium. They come in several commercial types, including martensitic, ferritic, austenitic, duplex, and precipitation-hardened varieties [10]. AISI 304 stainless steel is particularly popular because to its outstanding formability [11]. Stainless steel is used in spacecraft, vehicles, and steamships to improve fuel economy [12-14]. Ferritic stainless steels with 11-30% chromium and small quantities of carbon, nitrogen, and nickel are very resistant to pitting, crevice, and stress corrosion cracking in chloride conditions [15]. Due to their strong corrosion resistance, alloy steels containing 16% chromium are extensively utilized in household products. Despite being primarily ferritic, the heat-affected zone (HAZ) forms martensite because to its high carbon concentration and lack of stabilizing components. This type of steel is frequently used in refrigerator cabinet panels, dishwasher linings, stove trim rings, element supports, fasteners, and chimney liners.

Dak and Pandey [16] discovered that dissimilar welding of martensitic P92 to austenitic AISI 304L produced a balanced microstructure with significant residual stress distribution, which influenced mechanical characteristics and joint performance. García-García discovered that welding TWIP steel to austenitic/duplex stainless steels twice resulted in refined microstructures, which improved tensile strength and toughness. Optimal welding conditions resulted in significant improvements in joint mechanical characteristics. Arun Mani et al. [17] explored CO_2 laser beam welding (LBW) to combine AISI 430 ferritic stainless steel (FSS) and AISI 304 austenitic stainless steel (ASS) plates, examining the microstructural characteristics. They discovered that the breadth of the heat-affected zone (HAZ) and weld zone was modified by welding speed and heat input. The best results were obtained at a welding speed of 100 cm/min and a heat input of 1500W in a helium environment. Rajput et al. [18] found that adjusting CO_2 laser beam welding settings greatly improved the mechanical characteristics of austenitic-ferritic stainless-steel joints. Their research emphasized the production of ferrite and martensite in the HAZ, as well as the optimal welding rates and heat inputs for increasing hardness and tensile strength. Khan et al. [19] found ferrite formation on the austenitic side and martensite with dual-phase ferrite on the ferritic side of the HAZ, resulting in localized microhardness owing to element redistribution. Durgutlu [20] discovered that welding 316L stainless steel under 1.5% H_2-Ar resulted in the highest tensile strength, while toughness increased with heat input. Arun Kumar et al. [21] investigated the mechanical characteristics of welded junctions in dissimilar alloy steels comprising molybdenum and chromium in metal tube form. Tsuchiya et al. [22] used tungsten inert gas (TIG) welding to connect SS316L (N) austenitic stainless steel (ASS) and discovered that the hardness in both the heat-affected zone (HAZ) and the weld zone was lower than in the base material. A tiny ferrite pool was discovered in the completely austenitic alloy in worked form [22].

In the examination of Gas Tungsten Arc Welding (GTAW) of AISI 304 and AISI 409 with various fillers, an austenitic-ferritic transition zone with grain coarsening in the ferritic region were observed. The use of Ni-based fillers resulted in the highest tensile strength, whereas the utilization of ferritic fillers caused the formation of brittle phases and weaker joints [23]. Alizadeh-Sh et al. [24] used resistance spot welding on AISI 430 stainless steel to evaluate tensile strength and classify heat-affected zones (HAZs) as high, medium, or low temperature. Sathiya et al. [25] examined how different friction welding settings affected the metallurgical and mechanical characteristics of AISI 430, discovering that tensile failures occurred in the weld zone even after grain refinement was accomplished. Bilgin et al. [26] used friction stir welding (FSW) on AISI 430 to reduce excessive grain development and prevent the creation of σ-phase in the fusion zone.

Joining dissimilar metals is difficult due to variations in thermomechanical and chemical characteristics, resulting in residual stress and corrosion. To address these obstacles, researchers must investigate the impact of welding settings on mechanical characteristics. Optimizing GMAW parameters for dissimilar steels revealed that specific voltage,

current, and travel speed settings significantly improve weld quality. Ideal values were identified to minimize defects and maximize tensile strength [27].

The penetration depth is affected by travel speed, arc voltage, chemical composition, and welding settings [28]. Increasing arc travel speed increases penetration depth, which influences corrosion resistance, microstructural characteristics, and precipitation in the heat-affected and weld zones of stainless steel [29]. Electron beam welding (EBW) produced a columnar dendritic fusion zone, and carbide precipitates formed at the grain boundaries. Strong welds with ductile fracture modes were produced by deep penetration, guaranteeing high tensile strength[30]

The geometry of the weld pool is critical in influencing the corrosion resistance and mechanical properties of the weld metal, hence choosing the ideal welding process parameters is critical to achieving the required weld pool geometry. Resistance spot welding of AISI 304 and AISI 409 resulted in a dendritic fusion zone with minimal intermetallic phase formation. The hardness was higher in the fusion zone but exhibited softening near the AISI 409 side [31]. The purpose of this study is to assess the effect of various welding conditions on the microstructural and mechanical properties of gas metal arc welded butt joints between two different stainless steels, AISI 430 ferritic stainless steel (FSS) and AISI 304 austenitic stainless steel (ASS), using ER308L filler metal. Voltage, welding current, and travel speed are all considered input characteristics, whereas microstructure, tensile strength, and hardness are assessed as outcome parameters. Weldment specimens were made, and the parameters' effects on penetration depth, bead width, joint composition, bead shape, and mechanical characteristics were investigated. The examination of bead geometry under various welding conditions is visually shown, indicating the best welding parameters. Experiments were carried out using Taguchi's L27 orthogonal array (OA) [32], and ANOVA [33] was used to determine the influence of different welding parameter combinations.

2. Experimental Setup

The GMAW process fuses metals by forming an electric arc between the workpieces and a continually supplied consumable welding electrode. A feeder draws the electrode wire from a reel and guides it into the welding flame using a contact tip. The welding arc focuses on the edges of the joined stainless-steel plates, making it easier to move molten metal from the electrode wire to the weld pool. A protective gas is used to screen both the electrode wire and the weld pool against air contamination [33].

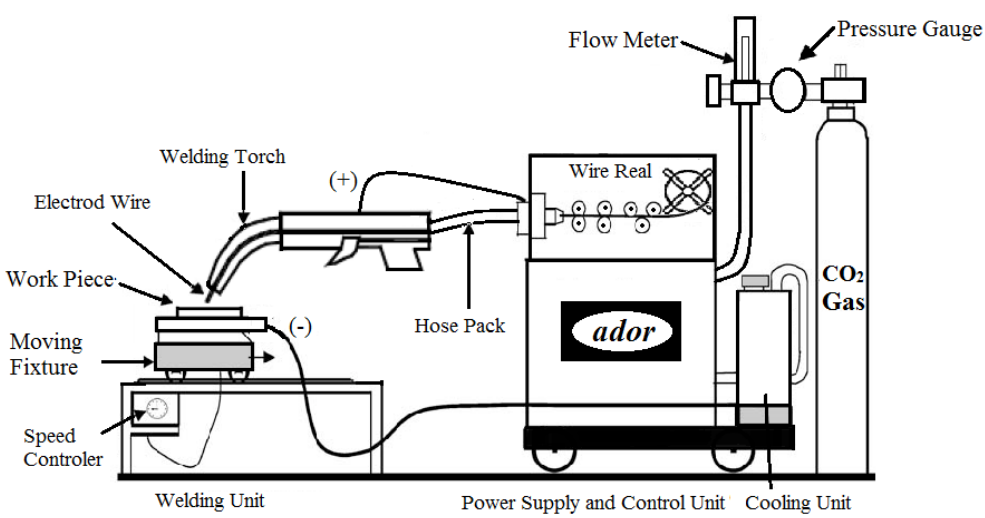

Fig. 1. Experimental setup of GMAW process.

2.1 Experimental-setup and procedure

Taguchi method's L27 orthogonal array, which consists of three columns and 27 rows, was used in the trials. The experimental design included three components, each with three levels. The rectangular samples, 50 mm wide, 200 mm long, and 4 mm thick, were welded in a butt arrangement using AISI 304 ASS and AISI 430 FSS plates. Figure

1 depicts the experimental setup, which included a CEMONT MT 251-type GMAW welding machine. In this investigation, CO_2 was used as shielding gas at a flow rate of 14 liters per minute. Two specimens from each plate were secured at a 45° bevel angle and welded using a 3 mm deep V-groove. Consumable wire (AISI 308L, 1.2 mm diameter) with 60° tip angle and DCEP was used for welding, as shown in Figure 2. After welding, both sides of the joint surfaces were cleaned with acetone to prevent distortion and eliminate rust, contaminants, and moisture. The welded specimens are shown in Figure 3. Table 1 displays the chemical composition of the base metal plates (AISI 304 ASS and AISI 430 FSS) with consumable filler wire (308L), while Table 2 details the mechanical properties of both steels.

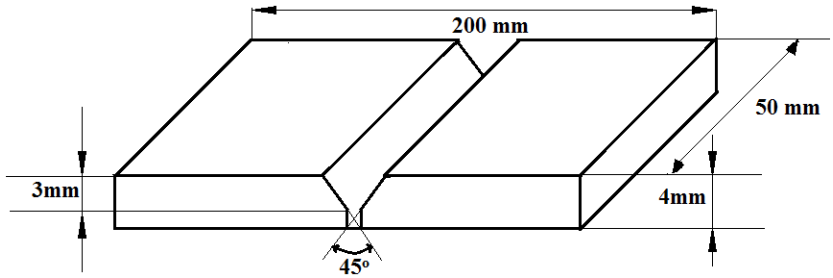

Fig 2. Sample with V- Groove

Table 1: Percentage chemical composition of base metal plates and electrode wire

Metals	Si	C	P	Cr	S	Mn	Ni
AISI 304	1.00	0.08	0.045	20.0	0.03	2.00	10
AISI 430	0.045	0.055	0.031	17.0	0.008	0.42	------
AISI 308L	1.00	0.03	0.045	19-21	0.02	2.00	10-12

Table 2: M echanical properties of base metals

Materials	Vicker's Microhardness	Yield Strength (MPa)	Tensile Strength (MPa)	%Elongation
AISI 304	182	295	590	55
AISI 430	170	345	517	25

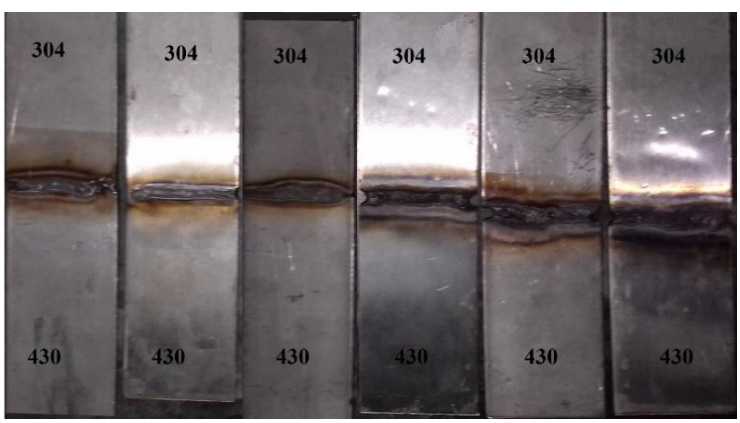

Fig. 3. Photographic view of the welded sample.

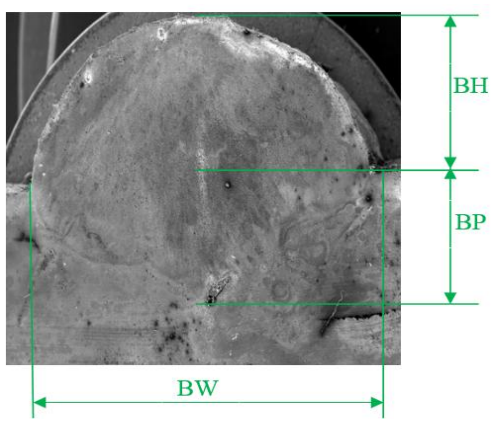

Fig 4. Bead profile of weld sample.

The bead profile of a small cutout from a welded junction is shown in Figure 4. The samples were machine polished (Econonet VH-1 MD, Chennai Metco, India) to a mirror-like sheen after being polished with emery paper with grits ranging from CW 400 to CW 2000. An aqueous solution containing equal parts of HNO3, HCl, and CH3COOH was used to etch each sample for one minute in order to improve the appearance of the microstructural characteristics. The elemental composition and microstructure were examined using a FESEM (SUPRA 55, Germany, equipped with Air Lock and EDS).

2. Results and Discussion

Table 3 presents the welding parameters together with their respective levels. Table 4 illustrates the Taguchi L27 orthogonal array, which outlines the experimental design. Table 4 lists the 27 experimental situations, including numerous control elements and their levels. Dittus-Boelter correlation:

Table 3: Control parameters with their levels

Symbol	Parameters	Levels		
A	Current (Amps)	150	170	190
B	Voltage (volt)	24	28	32
C	Speed (cm/min.)	20	40	60

The Taguchi method was used to improve performance characteristics by selecting the best parameter combinations from an L27 orthogonal array design of tests. Several studies were carried out using various parameters, including arc voltage, welding current, and speed. Hardness, penetration depth, and bead width were measured, and each sample's microstructure was studied. The next subsections show graphically how changing welding parameters affects penetration depth and bead width.

2.1 Penetration vs. Welding parameters

Figure 6 depicts the differences in penetration depth at various welding rates and currents. The graph demonstrates that, with constant current and voltage, penetration depth increases with welding speed. The maximum penetration depth is 3.451 mm when welding at 40 cm/min with a voltage of 32V and current of 190A. The minimal penetration depth of 2.19 mm is achieved with a voltage of 24V, a current of 150A, and a welding speed of 20 cm/min.

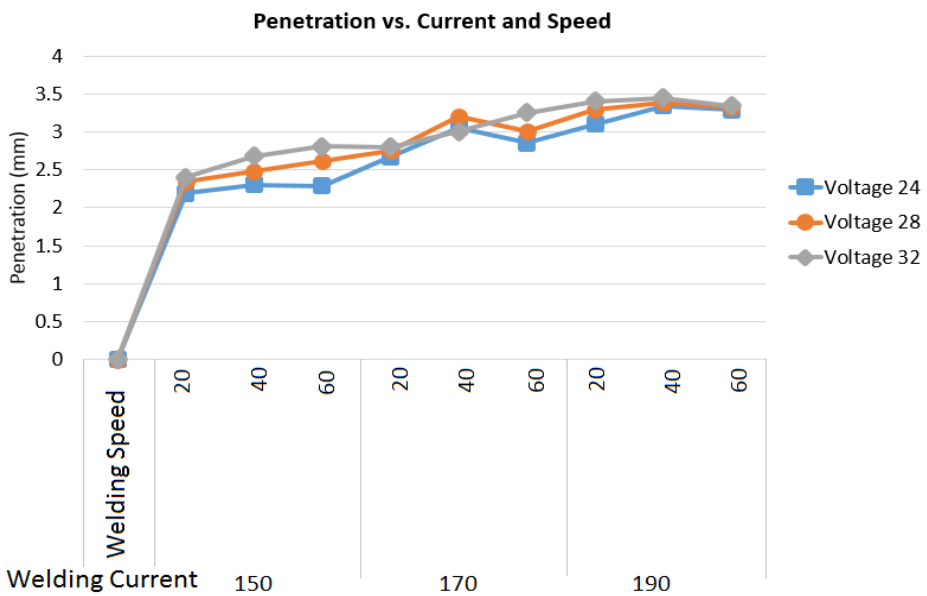

Fig. 6. Effect of welding current and travel speed on penetration

2.2. Bead width vs. welding parameters

Figure 7 illustrates variations in bead width across different welding speeds and currents. The graph illustrates how bead width varies with three distinct welding parameter settings. With a constant current of 190A and a voltage of 32V, the bead width grows as the welding speed increases. The maximum bead width of 10.35 mm is obtained with a welding speed of 60 cm/min, a voltage of 32V, and a current of 190A. In contrast, the lowest bead width of 9.675 mm is achieved at a welding speed of 20 cm/min, a voltage of 24V, and a current of 150A.

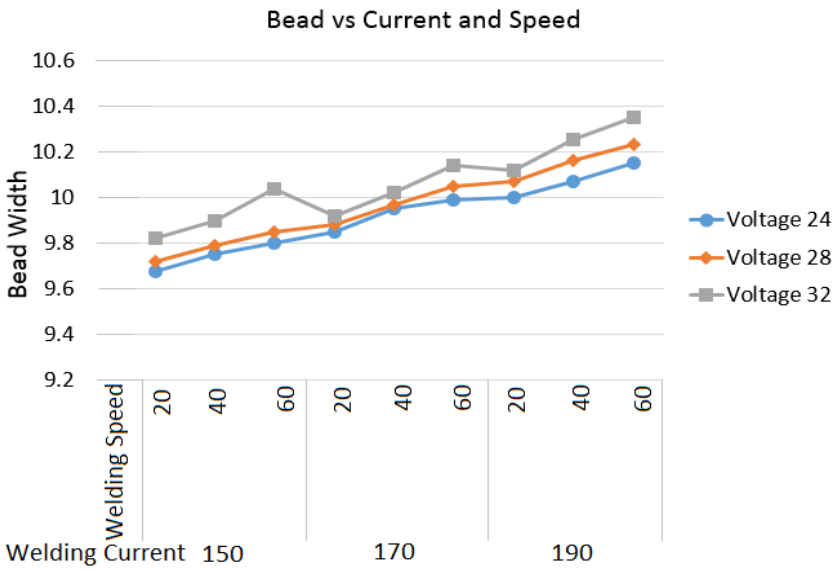

Fig. 7. Effect of welding current and travel speed on bead width

2.3 ANOVA

Variance is a critical statistical parameter for assessing experimental results, which is calculated using basic statistical tests. The analysis was conducted out at a 95% confidence level and a 5% significance level. If the p-value is below 0.05, it means that the relevant process parameters have a significant impact on the outcomes. MINITAB software was used in this experiment. As indicated in Tables 4 and 5, welding voltage is the most important factor determining penetration, with p-values less than 0.05. In contrast, welding speed and current have little impact on penetration.

Table 4: ANOVA result for Penetration

Source	DOF	Adj MS	Adj SS	P	F	% of Elements
1	2	1.7062	3.4123	0.000	55.76	82.29
2	2	0.119	0.237	0.493	0.73	5.72
3	2	0.129	0.259	0.462	0.80	6.25
Error	20	0.01194	0.2387			5.75
total	26		4.147			100

Table 5: Analysis of variance for Weld Width

Source	DOF	Adj SS	Adj MS	F	P	% of Elements
1	2	0.0995	0.0498	1.78	0.190	12.92
2	2	0.5215	0.2607	25.20	0.000	67.75
3	2	0.1325	0.0663	2.50	0.104	17.21
Error	20	0.0163	0.000815			2.12
Total	26	0.7698				100

Tables 6 and 7 demonstrate that welding current has a substantial effect on weld zone hardness and ultimate tensile strength, as evidenced by p-values < 0.05. Other process parameters have no substantial effect on weld zone hardness or ultimate tensile strength.

Table 6: Results of the ANOVA for Weld Zone Hardness

Source	DOF	Adj SS	Adj MS	F	P	(%) contribution
1	2	2232	1116	5.16	0.014	30.06
2	2	1109	554	2.11	0.144	14.94
3	2	525	262	0.91	0.415	8.32
Error	20	3559	178.0			46.68
Total	26	7425				100

Table 7: Results of the ANOVA for Tensile Strength

Source	DOF	Adj SS	Adj MS	F	P	(%) contribution
1	2	81606	40803	91.24	0.000	88.38
2	2	471	235	0.06	0.940	.51
3	2	2483	1241	0.33	0.721	2.68
Error	20	7779	389			8.43
Total	26	92339				100

2.4 Microstructure examination

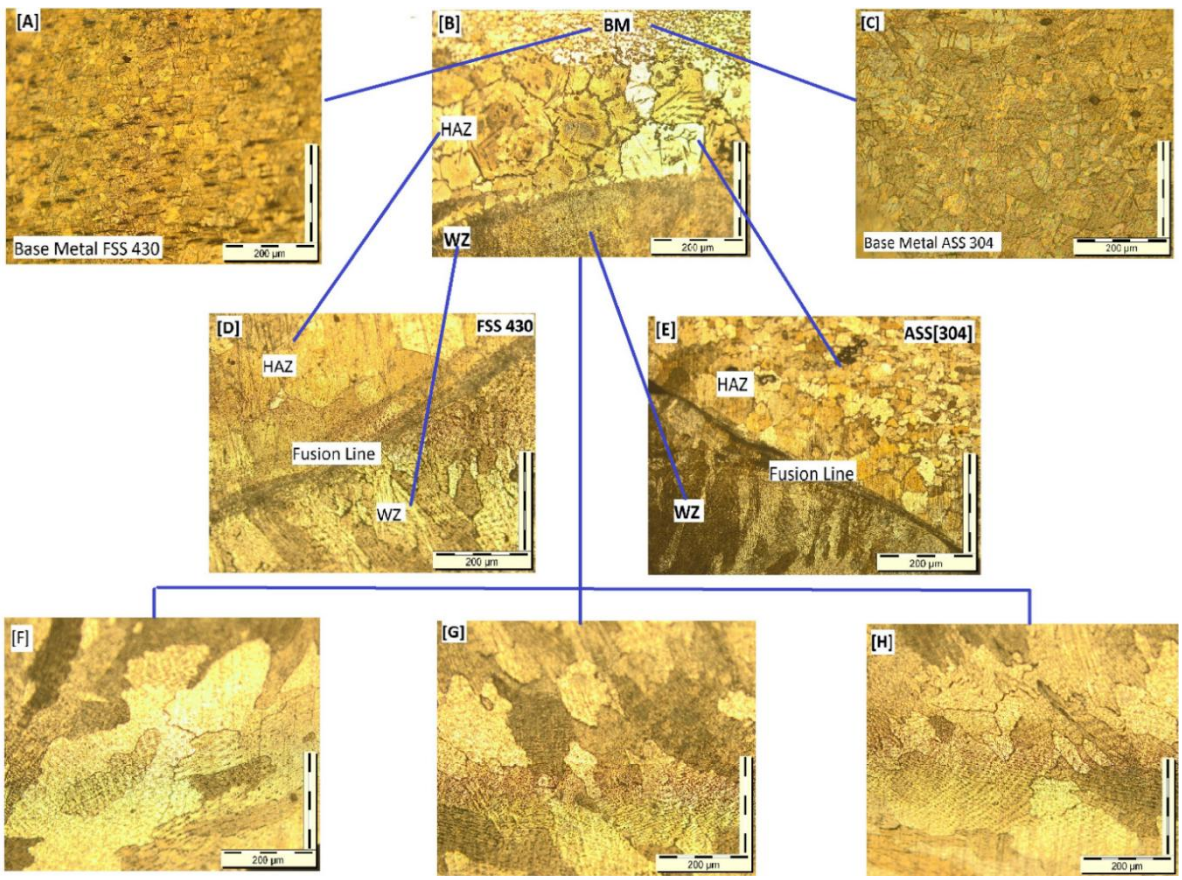

Fig. 7. Images of samples (A) Microstructure of AISI 430 (B) Interface microstructure of BM to WZ obtained, (C) Microstructure of AISI 304 (D and E) Three distinct areas (HAZ, FL and WZ) of BMs (F,G and H) Microstructures of weldments.

The microstructure of the welded joints was examined using a light optical microscope. Figure 7 Microstructural observations described martensite formation in the weld zone and showed refined grains at high welding speeds [30,31]. Welding factors have altered microstructural characteristics and grain size. Figures 7(D) and 7(E) clearly show three unique regions: HAZ, Weld Zone (WZ) and Fusion Line.

In each weld joint, the most sensitive location of the HAZ has more prominent grain boundary thickening than the HAZ closer to the Fusion Line (FL). Grain coarsening occurs on both sides of the weld contact in AISI 430 FSS and AISI 304 ASS plates. The results show that welding input factors have a considerable influence on the microstructure. Figures 7 (F, G and H) depict the microstructures of welded samples at a continuous welding current of 190A and an arc voltage of 32V, with welding speeds of 20, 40 and 60 cm/min. The findings show that grain boundary diameters decrease as welding speed increases, with the smallest grain boundaries found at 60 cm/min, resulting in the development of martensite.

2.5 Test for Micro-Hardness

Figure 8 depicts the microhardness values measured across the weldment cross-sections. Variations in welding parameters resulted in reduced hardness in the heat-affected zone (HAZ) and base metal when compared to the welded zone. Cr reduction near the fusion boundary caused localized hardness changes [31]. Higher arc voltage and welding current improved micro-hardness by forming austenitic or ferritic phases in the weld zone of 304 and 430 steels. Rapid chilling increased microhardness by refining grains and induced precipitation hardening. The weld zone had higher hardness than the HAZ, which contained coarser granules. Fine grains, martensite, and elements such as Cr and Ni all contributed to the weld zone having a higher micro-hardness than the base metal.

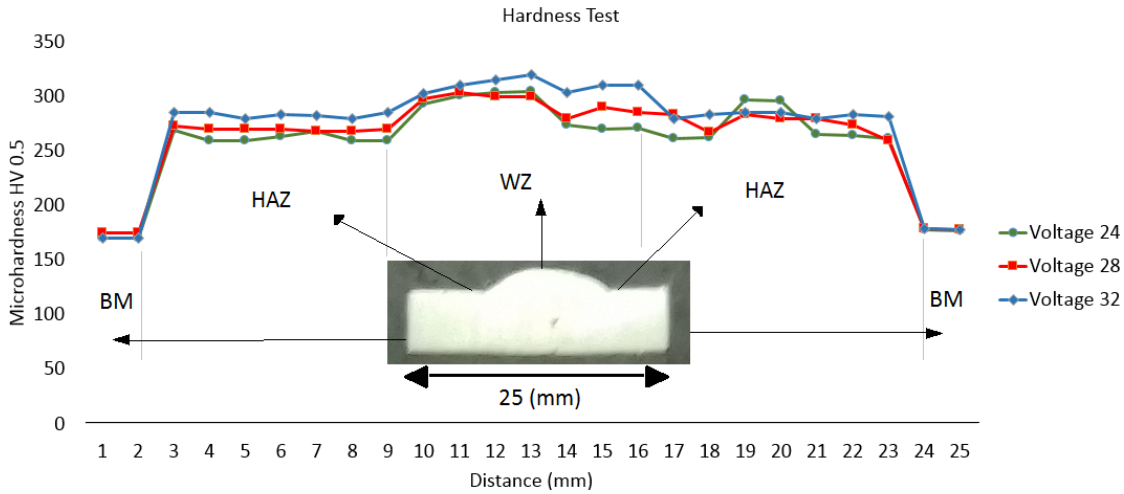

Fig 8. Values of Micro hardness at different arc voltages and distances from center of weld zone

2.6 X-ray Diffraction (XRD) and Energy Dispersive Spectroscopy (EDS) Analysis

Figure 9 shows the elemental composition of the welded zone, which includes Fe, Si, Cr, C, Ni, Mn and O as determined by EDS analysis. The study analyzed element diffusion within 200 µm from the 430 FSS to the 304 ASS base metal zone, indicating 19.20% Chromium, 4.52% Carbon and 6.31% Nickel. AISI 304 ASS is stabilized due to its high Ni and Cr content, which indorses a face-centered cubic (FCC) austenitic structure. In comparison, AISI 430 FCC has a body-centered cubic (BCC) structure due to its high Cr content and absence of Ni. The dilution of Ni from AISI 304 by AISI 430 reduces the stability of the austenitic phase, increasing the susceptibility to martensitic transformation upon rapid cooling at weld zone.The interaction between CO2 shielding gas and the weld pool causes oxidation, resulting in inclusions and depletion of specific alloy components.

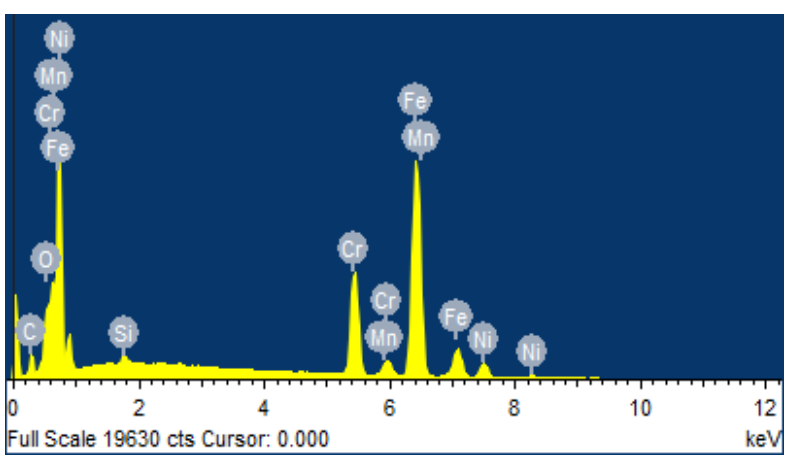

Fig. 9. EDS analysis of AISI 430/304 welded zone.

X-ray diffraction (XRD) examination was performed using a 2θ scanning angle to detect the phases present. The findings revealed Fe-rich compounds, including (hkl) phases 110, 200, 211 and 220 planes of martensite. Figure 10 depicts the peaks at 44.88°, 65.346° and 82.062°, and 99.521° correspond to the crystallographic planes 110, 200, 211 and 220 respectively, which show the presence of martensitic structures in stainless steel. Peak at 44.88° indicating that martensite is the dominant phase in the weld seam. Presence of additional peaks further supports the formation of martensite due to the rapid cooling during welding [25,31]. The change of austenite or ferrite to martensite influences the mechanical properties of the weld, increasing hardness and strength but also making it more brittle [30]. The martensite phase, defined by fine-grain microstructures within the weldments, is also visible.

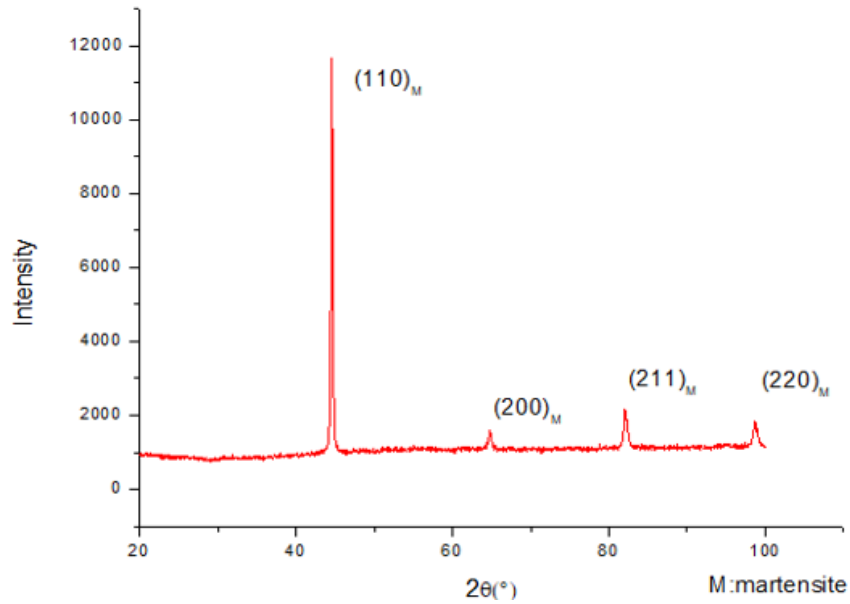

Fig. 10. X-ray diffraction diagram of weld seam.

2.7 Tensile test

Present paper shows higher tensile strength using GMAW compared resistance spot welding [31]. Figure 11 exhibits a sample after undergoing a tensile test, and Table 3 shows the results for different welding settings. The ultimate tensile strength of the welded samples varies from 410.2 MPa to 630.7 MPa, depending on the welding settings employed. The SS 304 samples had the highest ultimate tensile strength, while the SS 430 samples had the lowest. Table 4 shows the maximum tensile strength and yield stress values for the two base metals. SS 304 samples had the largest percentage elongation, whereas SS 430 samples exhibited the lowest. Table 8 presents the maximum ultimate tensile and yield strength values for each condition evaluated. Tensile strength analysis revealed that failures occurred in both the base metal and weld zones, depending on the welding conditions. The analysis of numerous parameter combinations indicates that optimal performance can be reached. Cracks were found in the 430-base material during the tensile test, indicating that the weld portions are stronger than the 304-base metal. This improved strength is most likely caused by the presence of chromium and nickel in the filler material.

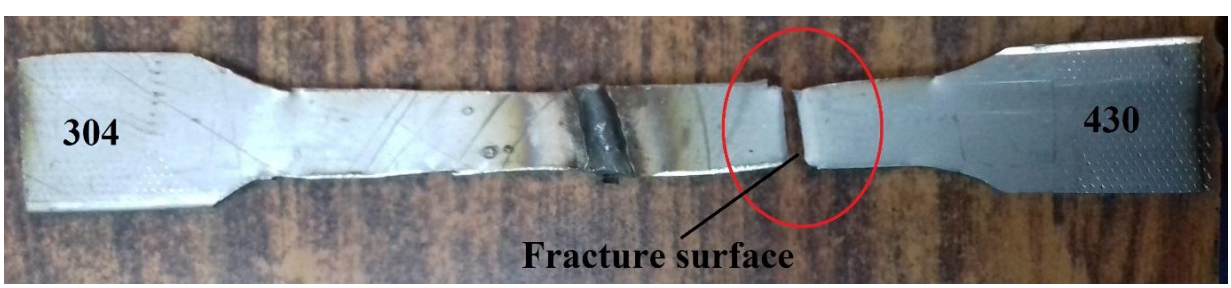

Fig. 11. Fracture surface after tensile test.

Table 8: Mechanical properties (MP) of welded samples

Weld samples	Yield Strength (MPa)	%Elongation	Tensile Strength (MPa)	Fracture location
S1	386.3	20.40	554.7	BM
S2	396.8	22.22	597.3	BM
S3	410.2	25.03	630.7	BM

Figure 12 depicts the surface cracks of weld samples after the tensile test. SEM examination of shattered surfaces from ferritic SS joints reveals the fracture morphology. Figure 12(a)-(b) shows fine dimples (FDs) and fracture formation in the base metal and weld zones. FDs are associated with ductility and strength, with finer dimples indicating greater ductility and strength. The coalescence of microvoids causes dimples in ductile fractures. Dimples on the weld zone (WZ) have a conical shape, whereas elliptical flat dimples are found on the base metal fracture surfaces. Impurities contribute to the creation of dimples, which range in size and dimension. Figure 12(b) shows that ideal parameters produce finer dimples than other welding settings.

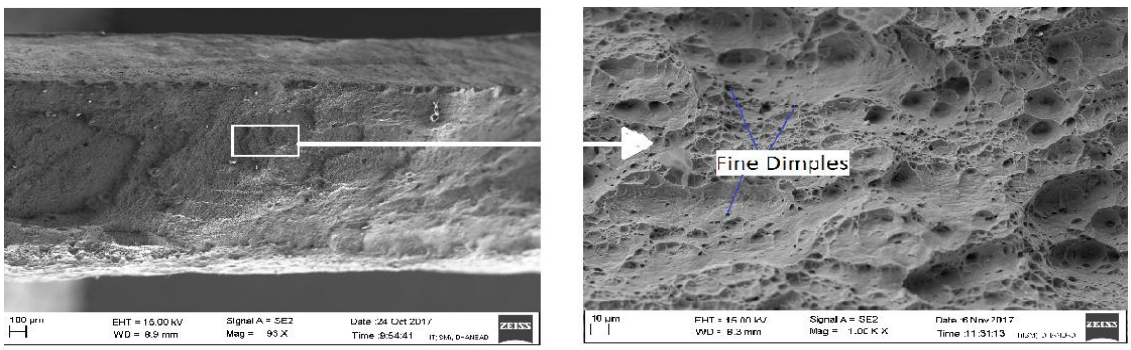

(a)

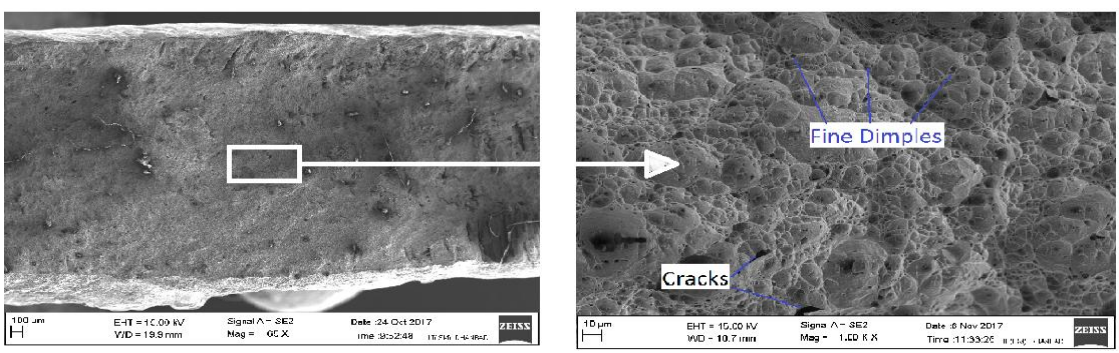

(b)

Fig. 12. The failure surface of (a) base metal (b) welding joint.

3. Conclusion

This study demonstrates the successful adjustment of Gas Metal Arc Welding parameters for combining AISI 304 austenitic stainless steel and AISI 430 ferritic stainless steel. By fine-tuning welding parameters like as current, voltage, and speed, the study improved tensile strength, microstructure, and bead quality. Furthermore, the impacts of filler metal and parameter modifications were studied, with XRD and EDS tests revealing the composition of materials within the weld. The key findings are stated below:

Microstructural Analysis: The investigation found microstructural variations between the parent metal, heat-affected zone (HAZ), and weld zone. The fusion and interaction of AISI 304 austenitic stainless steel (ASS) with AISI 430 ferritic stainless steel (FSS) resulted in unique microstructures in the weld zone that differed from the parent materials.

The weld zone revealed a refined grain structure due to rapid solidification. The heat-affected zone (HAZ) presented coarsening of grains, with a clear changeover from ferrite to austenite. Higher welding speed resulted in finer grains and enhanced microstructural stability [23,30,31]

Mechanical Properties:

- Tensile Strength: The findings reveal that the highest tensile strength was achieved with a welding current of 170 amps, a voltage of 32 volts, and a welding speed of 20 meters per minute. This combination yielded the best ultimate tensile strength, indicating a well-balanced weld quality. The presence of nickel and chromium in filler metal improved the mechanical strength.
- Hardness: The study indicated that the weld zone exhibited a higher hardness than both the base metal and the HAZ. Rapid cooling provided precipitation hardening and grain refinement it the weld zone. The most optimal welding parameter situation for maximum hardness were determined to be 170 amps, 28 volts, and a welding speed of 40 meters per minute.
- *Penetration Depth and Bead Width:* Increased welding speed at constant current and voltage led to deeper penetration. The ideal welding parameters for penetration and bead width were 190 amps, 32 volts, and a speed of 40-60 m/min. GMAW showed penetration depths comparable to resistance spot welding ([23,31]) but was lower than Electron Beam Welding (EBW) [30].

Taguchi and ANOVA Methodologies: The study used the Taguchi method with an L27 orthogonal array and ANOVA to optimize welding settings. This method successfully determined the optimal combination of welding settings for enhancing mechanical qualities like as tensile strength, hardness and bead quality.

Signal-to-Noise Ratio Analysis: The analysis identified certain parameter combinations that produced ideal weld characteristics. For example, the best outcomes for penetration, bead width and hardness were linked to specified values of current, voltage and welding speed.

The study effectively shown that by carefully adjusting GMAW parameters, it is possible to produce high-quality welds between different stainless steels with optimum mechanical properties and microstructural stability. The findings provide insight into the optimal settings for industrial applications employing such material combinations.

References

[1] Wang X, Kuaishe W. Microstructure and properties of friction stir butt-welded AZ31 magnesium alloy. Materials Science and Engineering A. 2006;431(1–2):114–117.

[2] Mai TA, Spowage AC. Characterisation of dissimilar joints in laser welding of steel–Kovar, copper–steel and copper–aluminium. Materials Science and Engineering A. 2004;374(1–2):224–233.

[3] Ghosh N, Pal PK, Nandi G. Gas metal arc welding dissimilar welding of AISI 409 ferritic stainless steel to AISI 316L austenitic stainless steel using AISI 308 filler wire. Engineering Science and Technology, an International Journal. 2017;20(4):1334–1341.

[4] Augustine C, George BP, Sudhish R. Parametric optimization of gas metal arc welding of dissimilar steels: duplex stainless steel 2205 and stainless steel 316L. International Journal on Theoretical and Applied Research in Mechanical Engineering. 2014;3:2319–3182.

[5] Olson DL, editor. ASM handbook: welding, brazing, and soldering. Volume 6. Materials Park (OH): ASM International; 1993. p. 322.

[6] Singla M, Singh D, Deepak D. Parametric optimization of gas metal arc welding processes by using factorial design approach. Journal of Minerals and Materials Characterization and Engineering. 2010;9(4):353–363.

[7] Nguyen TC, Weckman DC, Johnson DA, Kerr HW. High speed fusion weld bead defects. Science and Technology of Welding and Joining. 2006;11(6):618–633.

[8] Kim IS, Son JS, Kim IG, Kim JY, Kim OS. A study on relationship between process variables and bead penetration for robotic CO_2 arc welding. Journal of Materials Processing Technology. 2003;136(1–3):139–145.

[9] Sathiya P, Aravindan S, Ajith PM, Arivazhagan B, Haq AN. Microstructural characteristics on bead-on-plate welding of AISI 904L super austenitic stainless steel using gas metal arc welding process. International Journal of Engineering, Science and Technology. 2010;2(6):1–10.

[10] Caligulu U, Taskin M, Kejanli H, Orhan A. Interface characterization of CO_2 laser welded austenitic stainless steel and low carbon steel couple. Industrial Lubrication and Tribology. 2012;64(4):196–207.

[11] Özyürek D. Effect of weld current and weld atmosphere on the resistance spot weldability of 304L austenitic stainless steel. Materials and Design. 2008;29(3):597–603.
[12] Qiu R, Satonaka S, Iwamoto C. Effect of interfacial reaction layer continuity on the tensile strength of resistance spot welded joints between aluminum alloy and steels. Materials and Design. 2009;30(9):3686–3689.
[13] Shi Y, Zhang H, Takehiro W, Tang J. Study on laser welding characteristics of dissimilar metals. Optics and Laser Engineering. 2010;48:732–736.
[14] Mathieu A, Shabadi R, Deschamps A, Suery M, Mattei S, Grevey D, Cicala E. Dissimilar material joining using laser: aluminum to steel using zinc-based filler wire. Optics and Laser Technology. 2007;39(3):652–661.
[15] Rajasekhar A, Reddy GM, Mohandas T, Murti VS. Influence of post-weld heat treatments on microstructure and mechanical properties of AISI 431 martensitic stainless steel friction welds. Materials Science and Technology. 2008;24(2):201–212.
[16] Dak G, Pandey C. Experimental investigation on microstructure, mechanical properties, and residual stresses of dissimilar welded joint of martensitic P92 and AISI 304L austenitic stainless steel. International Journal of Pressure Vessels and Piping. 2021;194:104536.
[17] Mani AA, Kumar TS, Chandrasekar M. Mechanical and metallurgical properties of dissimilar welded components of AISI 430 ferritic and AISI 304 austenitic stainless steels by CO_2 laser beam welding. Journal of Chemical and Pharmaceutical Sciences. 2015;974:2115.
[18] Rajput SK, Kumar A, Tripathi SS, Sachan E. Investigation of microstructural behavior and mechanical properties of dissimilar weld joints of austenitic–ferritic stainless steel. Materials Today: Proceedings. 2020;25:778–784.
[19] Khan MM, Romoli L, Fiaschi M, Dini G, Sarri F. Laser beam welding of dissimilar stainless steels in a fillet joint configuration. Journal of Materials Processing Technology. 2012;212(4):856–867.
[20] Durgutlu A. Experimental investigation of the effect of hydrogen in argon as a shielding gas on tungsten inert gas welding of austenitic stainless steel. Materials and Design. 2004;25(1):19–23.
[21] Arunkumar N, Duraisamy P, Veeramanikandan S. Evaluation of mechanical properties of dissimilar metal tube welded joints using inert gas welding. International Journal of Engineering Research and Applications. 2012;2(5):1709–1717.
[22] Tsuchiya K, Kawamura H, Kalinin G. Re-weldability tests of irradiated austenitic stainless steel by a tungsten inert gas welding method. Journal of Nuclear Materials. 2000;283:1210–1214.
[23] Shojaati M, Beidokhti B. Characterization of AISI 304 and AISI 409 stainless steel joints using different filler materials. Construction and Building Materials. 2017;147:608–615.
[24] Welding Handbook. Metals and their weldability. 7th ed. Volume 4. Miami (FL): American Welding Society; 1982. p. 100–102.
[25] Alizadeh-Sh MA, Marashi SP, Pouranvari M. Resistance spot welding of AISI 430 ferritic stainless steel: phase transformations and mechanical properties. Materials and Design. 2014;56:258–263.
[26] Bilgin MB, Meran C. Effect of tool rotational and traverse speed on friction stir weldability of AISI 430 ferritic stainless steel. Materials and Design. 2012;33:376–383.
[27] Tesfaye FK. Parameter optimization of gas metal arc welding process for welding dissimilar steels. American Journal of Mechanical and Industrial Engineering. 2023;8(1):1–6.
[28] Shirali AA, Mills KC. Effect of welding parameters on penetration in gas tungsten arc welds. Welding Journal. 1993;72:347S–352S.
[29] Heino S, Knutson-Wedel EM, Karlsson B. Precipitation behaviour in heat affected zone of welded super austenitic stainless steel. Materials Science and Technology. 1999;15(1):101–108.
[30] Doomra A, Singh B, Sandhu SS. Weldability studies of AISI 409 ferritic stainless steel thick plates using electron beam welding process. International Journal of Manufacturing, Materials, and Mechanical Engineering. 2021;11(2):55–67.
[31] Safari M, Mostaan H, Ghaderi A. Dissimilar resistance spot welding of AISI 304 and AISI 409 stainless steels: mechanical properties and microstructural evolutions. Metallurgical Research and Technology. 2018;115(6):610.
[32] Roy RK. Design of experiments using the Taguchi approach: 16 steps to product and process improvement. New York: John Wiley and Sons; 2001.
[33] Rao RV. Modeling and optimization of gas metal arc welding process. In: Computational methods for optimizing manufacturing technology: models and techniques. Hershey (PA): IGI Global; 2012. p. 339–367.